

Progress Report for 3rd Quarter, NOV 2017- JAN 2018

OCT Image Analysis System for Grading and Diagnosis of Retinal Diseases and its Integration in i-Hospital

Milestone 1: Detection of macular edema

INTRODUCTION

Human retina mainly consists of two regions i.e. the macular and the ocular region. Macular region is where the vision is formed. Maculopathy tends to damage the macular region resulting in vision loss or even blindness. The two major macular syndromes are ME and CSR. ME is mainly found in diabetic patients where the retinal blood vessels become thinned because of hyperglycemia and leak proteins or other fluid deposits within retinal layers. CSR is caused due to leakage of serous within retinal pigment epithelium (RPE) layer. In the case of CSR, the neurosensory retina remains in contact while it is distorted in the case of ME. ME is clinically graded into two stages depending upon the severity of retinal thickness as defined by the study of early treatment diabetic retinopathy (ETDRS) [1]. Edema within the diameter of 500 micrometers centered at fovea is considered to be severe because it significantly causes vision loss or blindness. This stage is termed as clinically significant macular edema (CSME). The retinal edema outside this limit is known as non-clinically significant macular edema (non-CSME). CSR is also graded into two stages. Usually serous accumulates under the neurosensory retina and this type of condition leads to Type I CSR. CSR due to RPE leakage [2] is known as Type II CSR. Fig. 1 depicts the increased foveal depth between retinal inner limiting membrane (ILM) and choroidal layer in case of diseased macular pathology as compared to healthy eye.

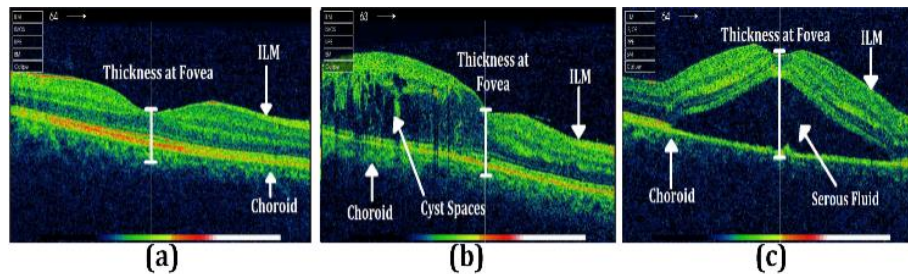


Fig. 1. Retinal OCT B-scans: (a) normal frame, (b) ME affected frame, (c) CSR affected frame.

Maculopathy can be identified through different testing techniques. The most commonly used techniques are fundography, fundus fluorescein angiography (FFA) and OCT. FFA is the best technique to visualize macular pathology however it is invasive and many people are allergic to the dye that is injected in the vein. OCT is the recently introduced technique that can objectively detect early syndromes of macular and ocular disorders. OCT is based on Michelson interferometer principle [3] and the major advantage of OCT over other techniques is that it can detect early symptoms of maculopathy

Different researchers have presented their findings about ME and CSR from OCT scans. Hannouche, R. Z. et al. [4] assessed fundography, bio-microscopy, FFA and OCT to detect diabetic foveal edema. They concluded that OCT can give objective evaluation about the severity of maculopathy as compared to other techniques. Zhang, W. et al. [5] proposed the use of OCT in the early treatment of diabetic macular edema (DME). Shrestha et al. [6] proposed the effective usage of OCT imaging in aligning the macula after ME surgery. Their study involved 60 patients. Mokwa, N. F. et al. [7] drew a comparison between OCT imaging technique, FFA and fundus photography (FP) for detecting exudative and non-exudative macular degeneration. They concluded that FP best indicates the RPE changes and drusen in case of age related macular degeneration (AMD). However, OCT is more sensitive in detecting minor changes in case of CNV. Helmy, Y. M. et al. [8] proposed classification of cystoid macular edema (CME) based on OCT findings in 104 eyes of 86 patients. They concluded that OCT provides better characterization of CME, and hence is very useful technique in quantitative measurement. Ferrara, D. et al. [9] identified the distinctive features of RPE and

choroid that appears in OCT scans of patients suffering from CSR. They considered 15 eyes of 13 patients in their study. Wani, J. S. et al. [10] diagnosed CSR from 48 eyes and concluded that OCT is an effective technique that can be used as a complement to FFA for the detection of CSR. Teke M. Y. et al. [11] compared FFA and OCT for evaluating the abnormalities in 100 CSR patients and they concluded that both techniques can help and back the clinicians to detect CSR. Ahlers, C. et al. [12] discussed the alteration in the retinal layers of CSR affected OCT scan. They studied 18 subjects of CSR and concluded that OCT imaging is more useful as it provides exact information regarding morphological changes along with retinal microstructure. Mitarai, K. et al. [13] found the changes at leakage points in CSR affected OCT scan. They included 26 subjects in their study out of which 23 were men and 3 were women and concluded that OCT noninvasively detects the morphologic alteration with much ease in the case of CSR

Some researchers have automatically detected ME using OCT images. Wilkins, G. R. et al. [14] identified the retinal fluid by annotating ILM and RPE and have evaluated their system on the dataset consisting of 16 eye patients. They achieved the average specificity of 96% and mean sensitivity of 91% for detecting retinal fluid. Sugruk, J. et al. [15] proposed an automated method for classifying diabetic macular edema (DME) and AMD subjects. For classifying DME subjects, they have extracted cyst segments with the accuracy of 86.6% while for detecting AMD, they clipped nerve fiber layer (NFL) from OCT scans to extract RPE and they achieved an accuracy of 100% for AMD subjects. Zhang, L. et al. [16] extracted inter-retinal layers for the diagnosis of cystoid macular edema (CME) through adaptive boosting. Their achieved accuracy was 98.6%. Srinivasan, P. P. et al. [17] proposed a fully automated SVM based method to detect DME, AMD and healthy subjects from retinal OCT scans. The accuracy of their proposed system was 100% for AMD cases, 100% for DME cases and 86.67% for healthy cases respectively. Recently Rashno, A. et al [18] proposed a fully automated neutrosophic transformation and graph based shortest path method to segment cyst regions from DME affected OCT scans however to the best of our knowledge there is no technical paper available that can automatically grade ME into CSME, non-CSME and CSR into Type-I CSR and Type-II CSR. Previously we have proposed fully automated robust system in [19] to diagnose ME, CSR or healthy pathology from 3D OCT volumes and here we propose an extension of [19] to automatically measure the severity of the disease by grading it to clinical standards through generated 3D retinal profiles. The proposed method is fully automated and is based on extracting 7 distinct features from the coherent tensors of OCT volumetric scans. These features were then fed to pair of SVM classifiers to automatically diagnose and grade CSR and ME retinal subjects. The major highlights are:

- We present a combined structure tensor graph searches (ST-GS) based segmentation framework that can automatically extract intra-retinal layers and fluid pathology from OCT images for the diagnosis of maculopathy.
- To the best of our knowledge, the proposed system is first of its kind that automatically extracts 3D retinal profiles of the ME and CSR subjects to measure the severity of the underlying disease and grades them as CSME, non-CSME, Type-I CSR and Type-II CSR clinical standards.
- It is worth noting that the automated 3D profiling and maculopathy grading by the proposed system is extremely fast and accurate. The proposed system takes one minute on average using 4th generation core i7 (1.8 GHz) processor with 8 GB RAM to generate 3D profiles and maculopathy grading reports.
- The performance of the proposed system was analyzed using receiver operator characteristics (ROC) parameters where the proposed system achieved the sensitivity, specificity and accuracy ratings of 96.77%, 100% and 97.78% respectively.

PROPOSED METHODOLOGY

The detailed block level diagram of a proposed framework is represented in Fig. 2. At first, an input OCT volumetric scan is loaded into the system where each B-scan is processed individually. Previously we have presented fully automated systems to diagnose maculopathy by extracting retinal layers through coherent structure tensor [19, 20, 21, 22]. But here, we present an extension of our existing framework that incorporates state of the art graph theory

for robust retinal layers tracing and extraction of cyst and serous fluid. The proposed system is divided into various stages. The first stage is the preprocessing stage in which the candidate B-scan is de-noised through adaptive low pass wiener filter. Afterwards, the proposed system computes coherent tensors to highlight retinal morphological structures. The candidate B-scan is then digitalized from which retinal layers are traced. In order to trace out intra-retinal layers from healthy and diseased B-scans, ST-GS decomposes the observed B-scan into an undirected graph where each pixel corresponds to a node and adjacent pixels are connected to each other via 4-neighbor connectivity. The retinal layers are then traced iteratively from the candidate graph by measuring the intensity variations in between connected nodes. The detailed description of proposed retinal tracing algorithm is presented in sub-section D. Furthermore, the proposed system also localizes cyst and serous pores by creating a retinal mask through extracted inner limiting membrane (ILM) and choroidal layer. After processing all the B-scans within OCT volume, the proposed system automatically reconstructs 3D retinal profiles from which 7 distinct features are extracted. These features are then fed to the multilayered SVM based decision support system to diagnose the pathological conditions of observed macula. If the candidate volumetric scan is diagnosed as having maculopathy symptoms then it is further graded as CSME, non-CSME, Type-I or Type-II CSR by measuring the disease severity from reconstructed surfaces. Detail description of each stage is explained in subsections below.

A. OCT Dataset Acquisition

The OCT dataset contains OCT volumetric scans of 90 subjects in which 54 were male and 36 were female. There are 11,520 B-scans within the dataset in which there are 3,840 healthy, 3,840 CSR and 3,840 ME affected B-scans. The dataset has been acquired using TOPCON 3D OCT 3000 machine from Armed Forces Institute of Ophthalmology (AFIO), Rawalpindi and all the scans are labeled by multiple expert ophthalmologists. Apart from scans labeling, the expert ophthalmologists also annotated the retinal layers as well based upon their experience in an isolated room. The detailed description about the dataset is tabulated in Table I.

Table I: Dataset Description

Subjects		Parameters	Type		
			Healthy	CSR	ME
Total Subjects	90	Frame Resolution (pixel x pixel)	951x 456	951x 456	951x 456
Male	54	Axial scans (pixels)	951	951	951
		B-scans in each volume	128	128	128
Female	36	Total Volumetric Scans	30	30	30
Mean Age	36.2	Total B-scans	3840	3840	3840
Acquired From		Armed Forces Institute of Ophthalmology (AFIO), Rawalpindi Pakistan			
Acquisition Machine		TOPCON 3D OCT 3000			

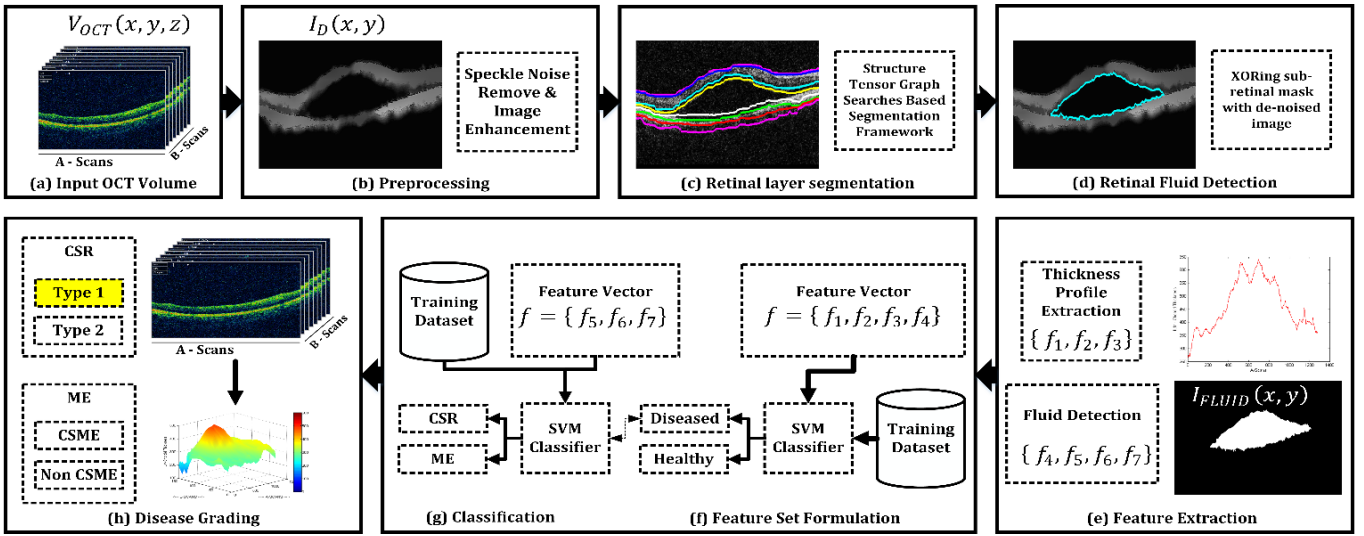


Fig. 2. Proposed methodology (a) input OCT volume (b) preprocessing stage (c) retinal layers and choroid segmentation (d) retinal fluid detection (e) feature extraction (f) feature vector formulation (g) classification (h) disease grading.

B. Preprocessing

In preprocessing stage, each frame within OCT volumetric scan $V_{OCT}(x, y, z)$ is enhanced to segment the retinal layers. At first, each frame of $V_{OCT}(x, y, z)$ is normalized and its green gray-scale channel $I_{Gray}(x, y)$ is kept for further processing. After that, different image enhancement techniques are applied to suppress the noise and to enhance the retinal pathology. The proposed system then uses an adaptive wiener filter to de-noise $I_{Gray}(x, y)$. Wiener filter adaptively de-noise the candidate image by measuring the neighborhood sparsity (centered at $I_D(u_i, v_j)$), as expressed in Eq. (1-3):

$$\Phi = \frac{1}{w_u w_v} \sum_{u_i \in w_u} \sum_{v_j \in w_v} I_{Gray}(u_i, v_j) \quad (1)$$

$$s^2 = \frac{1}{w_u w_v} \sum_{u_i \in w_u} \sum_{v_j \in w_v} I_{Gray}^2(u_i, v_j) - \Phi^2 \quad (2)$$

$$I_D(u_i, v_j) = \Phi + \frac{s^2 - \varepsilon^2}{s^2} (I(u_i, v_j) - \Phi) \quad (3)$$

where $I_D(u_i, v_j)$ represents an enhanced pixel, w_u are the vertical pixel within the window, w_v are the horizontal pixel within the window, Φ is the estimated mean within the defined neighborhood, s^2 is the estimated variance within the defined neighborhood and ε^2 represents the mean value of localized estimated variances [23]. After preprocessing, $I_D(x, y)$ is digitalized into $I_B(x, y)$ for further processing as shown in Fig. 3.

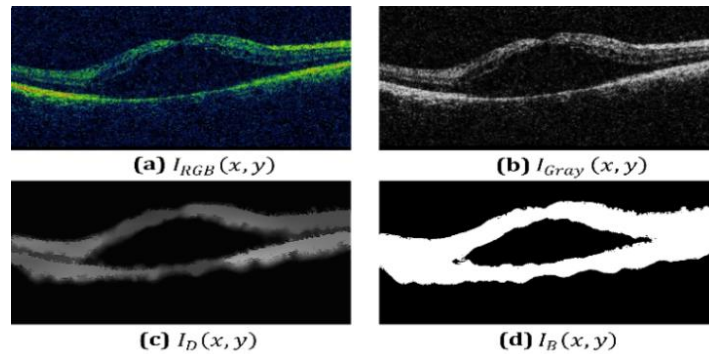


Fig. 3. Preprocessing stage (a) 3-channelled OCT image $I_{RGB}(x, y)$, (b) gray-scale image $I_{Gray}(x, y)$, (c) de-noised image $I_D(x, y)$, (d) digitalized image $I_B(x, y)$ text with descriptions of (a), (b), and (c).

C. Retinal Layers Segmentation

We propose a structure tensor graph searches (ST-GS) based segmentation framework for extracting intra-retinal layers from OCT scans. ST-GS is divided into two phases. First of all, the proposed framework generates a 2×2 structure tensor grid $S_2(x, y)$ to extract retinal layers from $I_D(x, y)$ and then retinal layers are extracted by decomposing $I_D(x, y)$ into an undirected graph. The coherent structure tensor grid $S_2(x, y)$ is generated by computing the partial gradients along orthogonal orientations and mathematically it is expressed in Eq. (4 to 7):

$$S_2(x, y) = \begin{bmatrix} F_X(x, y)^2 & F_X(x, y)F_Y(x, y) \\ F_Y(x, y)F_X(x, y) & F_Y(x, y)^2 \end{bmatrix} \quad (4)$$

$$(F_X(x, y))^2 = \sum_{x_i \in \varphi_x} \sum_{y_j \in \varphi_j} w(x_i, y_j) F_{\varphi X} \quad (5)$$

$$F_X(x, y)F_Y(x, y) = F_Y(x, y)F_X(x, y) = \sum_{x_i \in \varphi_x} \sum_{y_j \in \varphi_j} w(x_i, y_j) F_{\varphi XY} \quad (6)$$

$$(F_Y(x, y))^2 = \sum_{x_i \in \varphi_x} \sum_{y_j \in \varphi_j} w(x_i, y_j) F_{\varphi Y} \quad (7)$$

where $S_2(x, y)$ is the second order tensor grid, $F_X(x, y)^2$ represents the square of horizontal image gradients, $F_X(x, y)F_Y(x, y)$ and $(F_Y(x, y)F_X(x, y))$ represents the product of horizontal and vertical gradients and $F_Y(x, y)^2$ represents the square of vertical image gradients [24] and $w(x, y)$ represents the localized Gaussian window for the defined neighborhood. $F_{\varphi Y}, F_{\varphi XY}, F_{\varphi X}$ represent the directional derivatives of the candidate de-noised scan within the specified neighborhood, also represented mathematically through Eq. (8-10):

$$F_{\varphi Y} = \left(I'_{D_Y}(x - x_i, y - y_j) \right)^2 \quad (8)$$

$$F_{\varphi XY} = \left(I'_{D_X}(x - x_i, y - y_j) \right) \left(I'_{D_Y}(x - x_i, y - y_j) \right) \quad (9)$$

$$F_{\varphi X} = \left(I'_{D_X}(x - x_i, y - y_j) \right)^2 \quad (10)$$

The amount of coherency in each tensor is determined by computing the difference of eigenvalues between image gradients and the defined smoothing window $w(x, y)$ as expressed in Eq. (11).

$$C_w = \left(\frac{\lambda_1 - \lambda_2}{\lambda_1 + \lambda_2} \right)^2 \quad (11)$$

where ' λ_1 ', ' λ_2 ' represents the eigenvalues for both gradients along x and y direction respectively. When both gradients are aligned, then the achieved coherency will be 1. $C_w = -1$ shows the alignment in opposite direction and when there is no major orientation then $C_w = 0$ [24].

After that, a highly coherent tensor $I_C(x, y)$ is selected from all four tensors, which is then digitalized $I_B(x, y)$ and thick edges are adjusted through morphological skeletonization.

D. Retinal Layers Tracing

After highlighting the retinal layers, ST-GS automatically traces each layer iteratively. The tracing algorithm works in a way that it first decomposes the candidate scab into an undirected graph where each pixel corresponds to a node and adjacent nodes are connected to each other via 4-neighbor connectivity. The algorithm then automatically initializes the seed points and generate binary map for each retinal layer. At each iteration, the seed points traverses to nearest node by measuring the intensity differences. If the intensity difference between two or more nodes is same then top seed points give priority to downward nodes. Similarly, the bottom seed points give priority to upward nodes. When the top or bottom seed point observe a transition between foreground and background pixel then they include that pixel into the respective layer map and change the foreground pixel to background. The whole algorithm converges when the initialized seed points becomes equal. Fig. 4. shows the retinal layers segmentation results on randomly selected CSR scan.

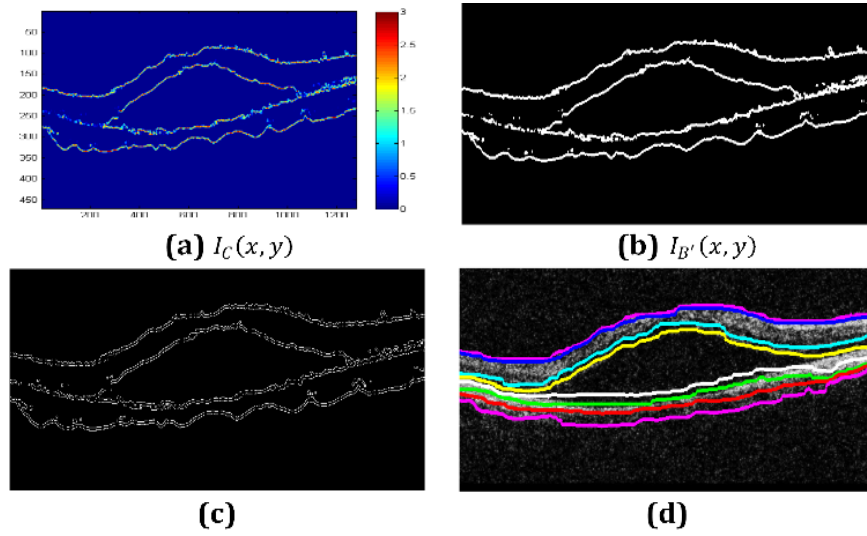


Fig. 4. Segmenting retinal and choroid layers (a) highly coherent 2D structure tensor ($I_C(x, y)$), (b) digitalized map $I_{B'}(x, y)$ of $I_C(x, y)$, (c) skeletonized retinal layers (d) segmented retinal layers.

Retinal layers segmented out from randomly selected 3 cases of CSR, healthy and ME subjects are shown in Fig. 5. It can be observed from Fig. 5. that in the case of healthy subjects, all retinal layers are closely intact whereas in the case of CSR and ME, retinal layers are detached due to cyst spaces in between them. Table II shows the axial scans (A-scans) mean separation between retinal layers of all 3 types of retinal disorders. It can be observed from the tabulated data that in case of healthy subjects, mean value for all retinal layers is less as compared to CSR and ME cases.

Table II: Retinal layers separation for all 3 types of retinal subjects

Layers	Healthy	CSR	ME
	Mean \pm S.D (μm)	Mean \pm S.D (μm)	Mean \pm S.D (μm)
ILM-GCL	36.789 \pm 6.2	67.248 \pm 10.29	84.215 \pm 14.71
GCL-INL	38.114 \pm 5.4	54.764 \pm 13.17	124.10 \pm 16.68
INL-OPL	40.028 \pm 8.1	42.857 \pm 8.76	115.738 \pm 15.92
OPL-ONL	32.582 \pm 5.8	248.168 \pm 32.64	201.612 \pm 24.09
ONL-OS	31.937 \pm 4.8	74.599 \pm 15.85	192.577 \pm 21.96
OS-RPE	32.743 \pm 2.7	60.008 \pm 15.08	108.349 \pm 14.79
RPE-CHOROID	31.327 \pm 9.2	64.386 \pm 9.78	96.47 \pm 17.63

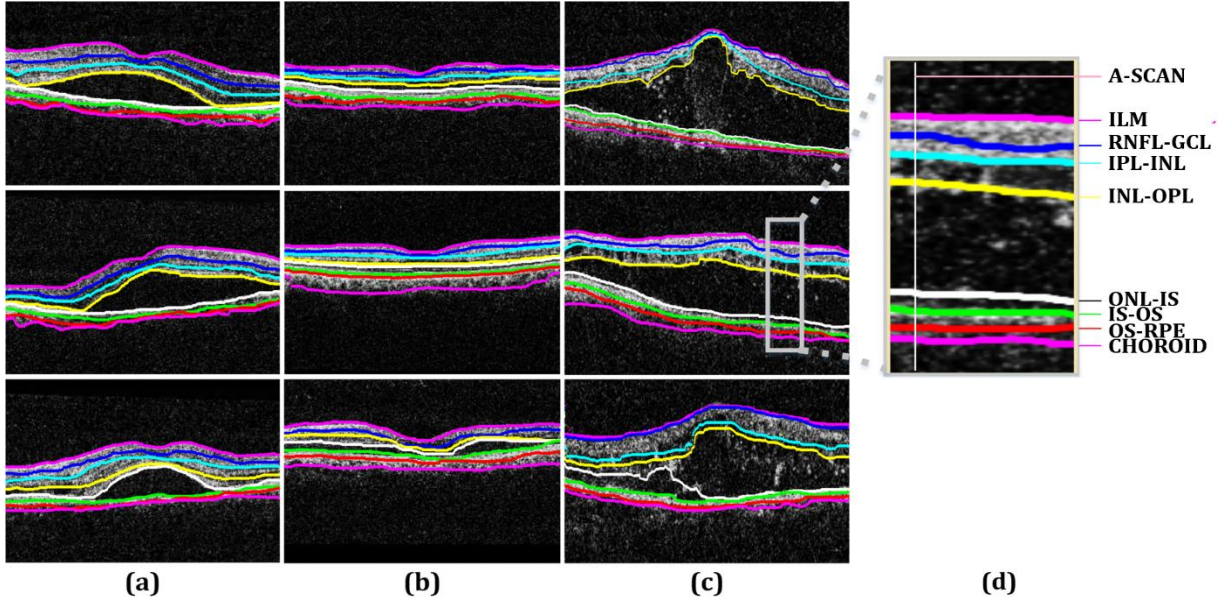


Fig. 5. Segmented Retinal Layers (a) CSR affected Frame, (b) Healthy Frame, (c) ME affected Frame, (d) Segmented Retinal Layers in one A-scan: ILM, Retinal Nerve Fiber Layer (RNFL)-Ganglion Cell Layer (GCL), Inner Plexiform Layer (IPL)-Inner Nuclear Layer (INL), INL-Outer Plexiform Layer (OPL), Outer Nuclear Layer (ONL)-Inner Segment (IS), IS-Outer Segment (OS), OS-Retinal Pigment Epithelium (RPE), Choroid.

E. Retinal Fluid Detection

After segmenting retinal layers, ILM and choroid are used to automatically extract fluid segments by creating a retinal mask $I_{Mask}(x, y)$. $I_{Mask}(x, y)$ is a binary map that is created by keeping all the pixels in between ILM and choroid as 1's and rest of the pixels as 0's. After creating a mask, it is logically fused with $I_B(x, y)$ to extract the fluid pathology as expressed in Eq. (12). Fig. 6 shows the extracted fluid segment for the randomly selected scan whereas the categorization of fluid pathology as cyst or serous is done by analyzing f_5 , f_6 and f_7 .

$$I_{FLUID}(x, y) = I_{Mask}(x, y) \oplus I_B(x, y) \quad (12)$$

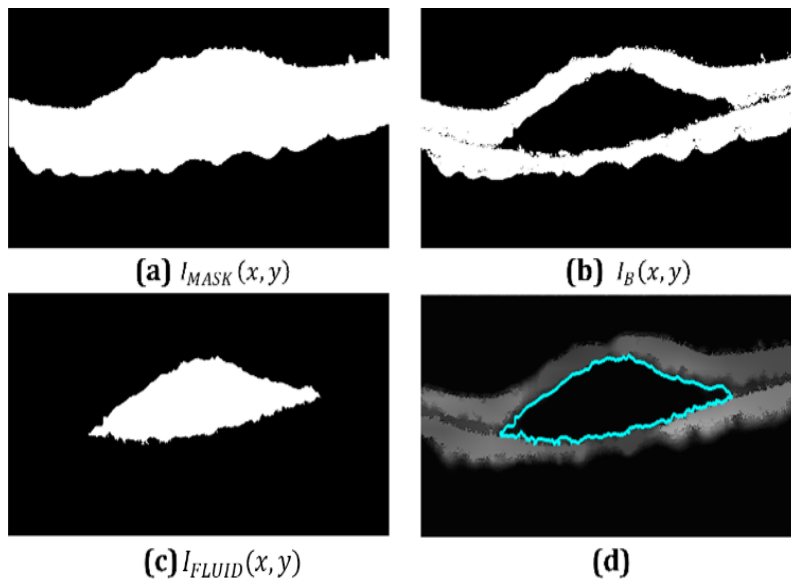


Fig. 6. Retinal Fluid Extraction: (a) retinal mask $I_{Mask}(x, y)$, (b) digitalized image $I_B(x, y)$, (c) fluid obtained through fusion of (a) and (b) (d) fluid mapped on $I_D(x, y)$.

F. Thickness Profile Extraction

In the proposed system, a retinal thickness profile for the processed B-scan is generated by extracting retinal layers from macular pathology as depicted in $I_B(x, y)$. In order to generate the thickness map T_{MN} , the absolute difference between ILM and choroid is computed as illustrated in Eq. (13-14):

$$T_{MN} = \begin{bmatrix} \tau_{11} & \cdots & \tau_{1N} \\ \vdots & \tau_{ij} & \vdots \\ \tau_{M1} & \cdots & \tau_{MN} \end{bmatrix} \quad (13)$$

where

$$\tau_{ij} = \left(\left| B_{i_{ILM}_j}(u, v) - B_{i_{Choroid}_j}(u, v) \right| \right) \quad (14)$$

' i ' ranges from 0 to 127 (total B-scans) and ' j ' is equal to total A-scans in each B-scan. This process is repeated for all the B-scan frames in $V_{OCT}(x, y, z)$ to reconstruct the 3D retinal thickness surface and fluid space cavity. Fig. 7 shows the reconstructed retinal surface from candidate volumetric scan.

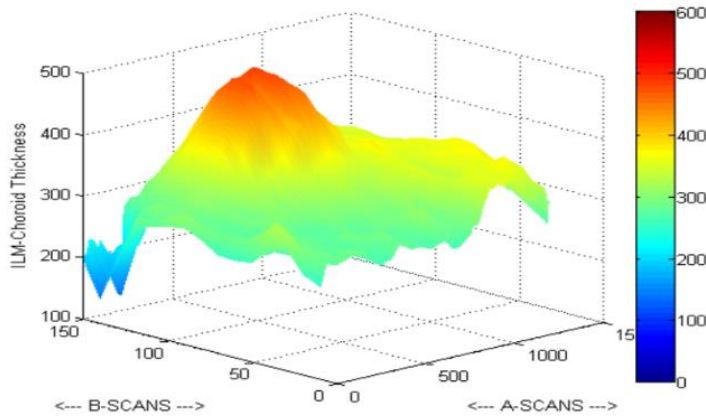


Fig. 7. 3D retinal thickness surface $R(x, y, z)$ formation.

Afterwards, the auto-generated retinal surface $R(x, y, z)$ is passed through the low pass Gaussian filter to suppress small sharp transitions. Eq. (15-16) represents the smoothing process of a retinal surface mathematically:

$$R_D(x, y, z) = \sum_{x_i \in w_x} \sum_{y_j \in w_y} \sum_{z_k \in w_z} \Delta * R(x_i, y_j, z_k) \quad (15)$$

$$\Delta = \frac{1}{\sqrt{(2\pi)^3 |\epsilon|}} e^{-\frac{1}{2}(x-\mu)^T \epsilon^{-1} (x-\mu)} \quad (16)$$

where μ is the mean value and ϵ is the covariance matrix.

G. Features Extraction

We have extracted 7 distinct features to automatically differentiate between ME, CSR and healthy subjects. The first 3 features are obtained from intra-retinal thickness profile and rest of the 4 features are obtained from fluid pores. These features were fused together to form 7D feature set $f = \{f_1, f_2, f_3, f_4, f_5, f_6, f_7\}$. Each feature that we extracted to distinguish between retinal subjects is discussed below:

Max Thickness (f_1): It is the peak point in the T_{MN} thickness map, which represents the highest difference between ILM and choroid as expressed in Eq. (17-18):

$$f_1 = \max[T_m] \quad m = 0,1,2 \dots M \quad (17)$$

$$f_1 = \max[|B_{m_{ILM}}(u,v) - B_{m_{Choroid}}(u,v)|] \quad (18)$$

Min Thickness (f_2): It is the shallowest point in the T_{MN} thickness map, which represents the lowest difference between ILM and choroid as expressed in Eq. (19-20):

$$f_2 = \min[T_m] \quad m = 0,1,2 \dots M \quad (19)$$

$$f_2 = \min[|B_{m_{ILM}}(u,v) - B_{m_{Choroid}}(u,v)|] \quad (20)$$

Absolute Thickness Variation (f_3): It depicts the variation within the macular profile due to the presence of fluid spaces and mathematically this variation is computed using Eq. (21):

$$f_3 = |f_2 - f_1| \quad (21)$$

Fluid Area (f_4): This feature determines the total cyst area within the macular region. It is computed using Eq. (22):

$$f_4 = \sum_{i=0}^{127} Area(I_{FLUID}^i(x,y)) \quad (22)$$

where $I_{FLUID}^i(x,y)$ represents the i^{th} fluid B-scan.

Fluid Boundaries Magnitude (f_5): This feature describes the strength of change in the fluid boundaries and it is computed using Eq. (23).

$$f_5 = mean\left(\sum_{i=0}^{127} \sqrt{\left(\frac{\partial I_{FLUID}^i(x,y)}{\partial x}\right)^2 + \left(\frac{\partial I_{FLUID}^i(x,y)}{\partial y}\right)^2}\right) \quad (23)$$

Mean of Fluid Orientation (f_6): This feature describes the orientation of fluid change and it is calculated using Eq. (24)

$$f_6 = mean\left(\sum_{i=0}^{127} \tan^{-1}\left(\frac{\frac{\partial I_{FLUID}^i(x,y)}{\partial y}}{\frac{\partial I_{FLUID}^i(x,y)}{\partial x}}\right)\right) \quad (24)$$

Fluid Segments Count (f_7): It is the total count of fluid segments present within macular region.

$$f_7 = \sum_{i=0}^{127} \sum_{k=1}^{\gamma} (I_{FLUID}^{i,k}(x,y)) \quad (25)$$

where γ denotes total fluid segments with a single B-scan.

Table III shows some of the features extracted from 5 randomly selected cases of each type along with the mean and standard deviation value of entire dataset. It can be observed from table III that all 7 features deviated more in case of diseased eyes as compared to healthy ones. This is due to increased fluid density across volumetric scans of ME and CSR affected eyes.

H. Classification

1. Validation of Proposed Classification Model

We have used support vector machines (SVM) based multilayered classification system to distinguish between three different pathological conditions of human retina [25]. The proposed system extracts 7 distinct features from auto-generated 3D retinal profiles and extracted fluid pathology then these features are fused together to form a 7D feature set $f = \{f_1, f_2, f_3, f_4, f_5, f_6, f_7\}$, passed to multilayered SVM classification model for the automated diagnosis of maculopathy. At first, the four features f_1, f_2, f_3, f_4 are passed to the classification model to diagnose candidate volumetric scan as healthy or diseased. If the candidate volumetric scan is classified as diseased then SVM further classifies it as ME or CSR using f_5, f_6, f_7 . The reason for using SVM based classification model is because it is fast [25] and it has high performance for binary classification tasks. Also, the SVM employed in the proposed classification system uses multilayer perceptron (MLP) and Gaussian Radial Basis Function (RBF) as kernel and it is hierarchical which means that at first it is used to diagnose candidate scan as healthy or diseased. If it is diagnosed as diseased then it is further classified as ME or CSR. The proposed system was trained on the set of 30 labeled OCT volumes. These training volumes are different from the 90 volumetric scans which were used for testing. The performance of the classification model in training phase was measured using k-fold cross validation where the value of 'k' was iterated from 2 to 10 in step of 2. The maximum accuracy is achieved for k equals to 10 as shown in Table IV and the respective trained model is chosen for classification.

Table III: Retinal layers separation for healthy and maculopathy subjects

Pathology	Subjects	Features						
		f_1 (mm)	f_2 (mm)	f_3 (mm)	f_4	f_5	f_6	f_8
Healthy	Subject 1	36.51	11.38	25.14	124.27	0.0024	1.39e-6	7
	Subject 2	39.69	23.02	16.67	140.28	0.0019	1.78e-6	2
	Subject 3	34.13	19.58	14.55	0.00	0	0	0
	Subject 4	50.54	32.54	17.99	126.71	0.0068	1.41e-6	4
	Subject 5	38.36	18.26	20.11	174.34	0.012	1.55e-6	1
	Mean	40.21	21.63	18.58	97.85	0.0027	1.15e-6	3.25
	S.D	5.66	6.91	3.60	59.31	0.0043	6.29e-7	2.48
CSR	Subject 1	64.29	38.10	26.19	11827.1	0.0096	7.18e-6	15
	Subject 2	82.02	42.33	39.69	20981.4	0.0091	9.31e-6	27
	Subject 3	68.79	34.66	34.13	22936.9	0.0064	9.87e-6	21
	Subject 4	63.50	43.39	20.11	8724.10	0.0085	6.92e-6	16
	Subject 5	71.70	35.98	35.72	26443.2	0.0077	9.98e-6	19
	Mean	69.65	39.62	30.03	16117.3	0.0084	8.32e-6	19.75
	S.D	6.68	3.43	7.05	6760.61	0.0011	1.33e-6	4.27
ME	Subject 1	72.23	36.25	35.98	7023.88	0.0058	1.26e-5	38
	Subject 2	48.42	25.66	22.75	18400.9	0.0068	3.56e-6	42
	Subject 3	49.48	21.96	27.52	14619.3	0.0062	3.74e-6	37
	Subject 4	62.18	33.07	29.10	27120.8	0.0076	1.32e-5	29
	Subject 5	65.62	39.42	26.19	5201.17	0.0051	2.72e-6	42
	Mean	58.07	29.23	28.83	16791.2	0.0066	8.28e-6	36.5
	S.D	9.27	6.52	4.37	7960.8	0.0008	4.70e-6	4.75

Table IV: Performance of Proposed Framework

Stage	K	Max Accuracy
Maculopathy Diagnosis	2	0.942
	4	0.957

Stage	K	Max Accuracy	
	8	0.968	
	10	0.980	Classification Model
	12	0.974	
Maculopathy Characterization	2	0.932	
	4	0.957	
	8	0.978	
	10	0.991	Classification Model
	12	0.987	

2. Retinal subject classification

After completion of a training phase, the proposed classification model was used to diagnose the unlabeled scans. For classifying the test candidate(s), a 7D feature vector is computed in a similar manner as discussed above and a prediction about the sample is obtained whether the processed scan is 'healthy', 'ME positive' or 'CSR positive'. The proposed algorithm for the classification of retinal subjects is shown in Fig. 8. Classifier's rating is measured by four parameters that are true positive (TP), false positive (FP), true negative (TN), and false negative (FN) given by the following relations in Eq. (26-28):

$$Accuracy = \frac{TP+TN}{TP+TN+FP+FN} \quad (26)$$

$$Sensitivity = \frac{TP}{TP+FN} \quad (27)$$

$$Specificity = \frac{TN}{TN+FP} \quad (28)$$

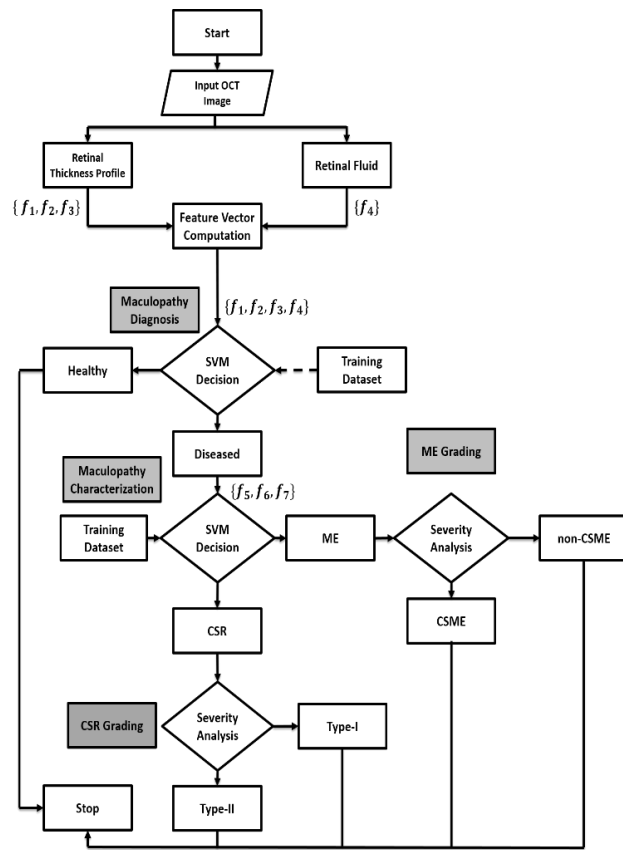


Fig. 8. Flowchart of classification algorithm.

I. Retinal Disease Grading

After extracting ILM and choroidal layers from all B-scans, a 3D retinal profile and fluid pathology is extracted which is used to screen the subject as healthy or diseased. The auto-generation of 3D retinal surfaces is also shown in Fig. 9 where the thickness range over 500 μm is shown in red color, range from 400 μm to 500 μm is shown in orange color and so on.

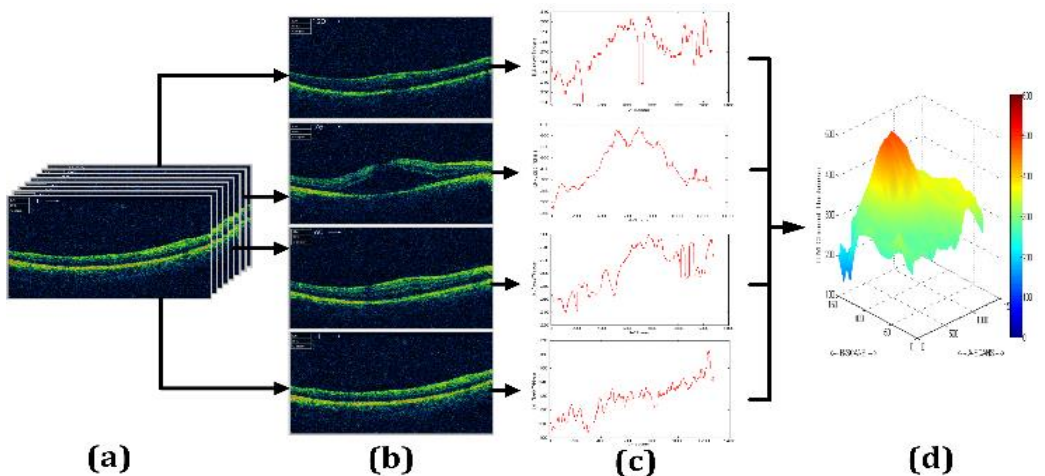


Fig. 9. 3D thickness heat map (a) Total B-scans of one case (b) 4 B-scans out of total B-scans (c) ILM - Choroid thickness plot for each B-scan in (b) (d) 3D thickness heat map of total B-scans.

If the subject is diagnosed as having maculopathy symptoms then the proposed system further grades it as per clinical standards. Auto-grading of ME as CSME or non-CSME is performed by measuring the cyst segments within

the foveal diameter of 5500 microns. If there are cyst segments within the foveal diameter of 5500 microns, then diagnosed ME is graded as CSME otherwise it is graded as non-CSME. In the case of CSR, when serous outbreaks neurosensory retina then it is graded as Type I CSR otherwise CSR due to RPE rupture is graded as Type II CSR. If the candidate subject is diagnosed as having CSR syndromes then the proposed system further grades it as Type-I or Type-II by measuring the density of serous along with its location with respect to RPE layer. If the serous grows above RPE then the diagnosed CSR is graded as Type-I otherwise it is graded as Type-II CSR. Fig. 10 shows the ME, CSR grading of 2 randomly selected subjects from each category and Table V shows the description of dataset which has been graded as per clinical standards by multiple expert ophthalmologists.

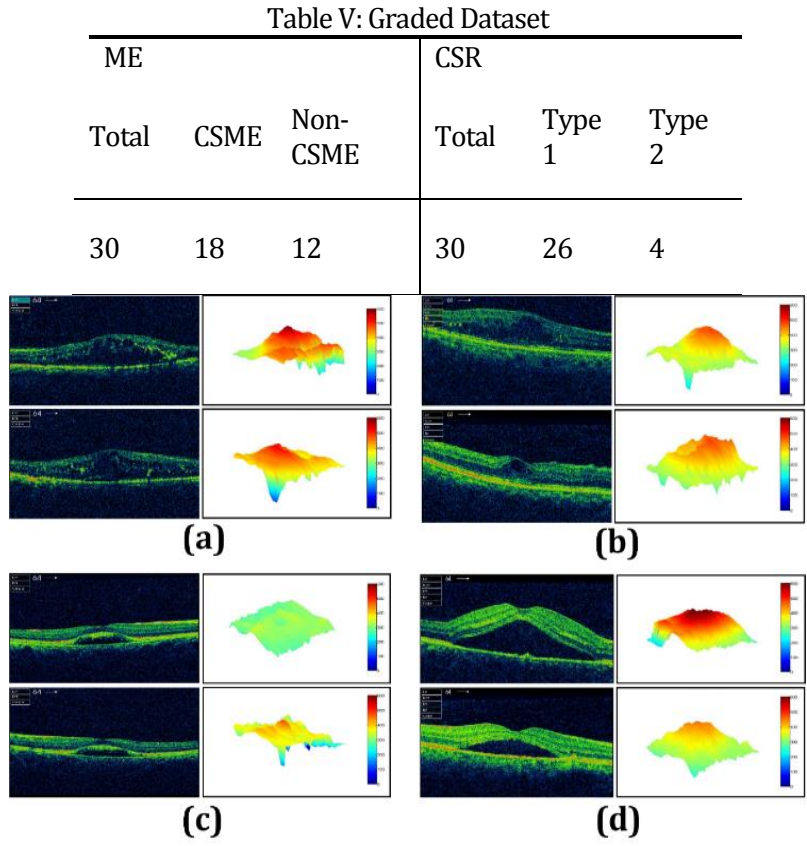


Fig. 10. Disease grading (a) CSME (b) non-CSME (c) Type II CSR (d) Type I CSR.

3. RESULTS

The proposed system was tested on the dataset that we acquired from AFIO, Rawalpindi Pakistan and it has been validated by multiple expert ophthalmologists. The dataset has overall 90 OCT volumetric scans in which 30 scans depict healthy pathology, 30 scans are of ME and the remaining 30 scans shows the CSR pathology. The proposed system was able to correctly predict all the diseased scans and 28/30 healthy scans. All the predictions have been cross validated by expert ophthalmologists and Table VI shows the overall performance of the proposed system.

Table VI: Achieved results

Type	Correctly Classified	Specificity	Sensitivity	Accuracy
ME	30 / 30			
CSR	30 / 30			
		100%	96.77%	97.78%
Healthy	28 / 30			

Furthermore, the ST-GS framework has been validated against manual annotations for different retinal pathologies by measuring the mean error rate. Mean error rates are computed by taking the absolute difference of ST-GS segmented layers from manual annotations and then taking their mean. Table VII shows the mean retinal layers segmentation error from five randomly selected samples of each category. Apart from this, the performance of the proposed system to automatically grade maculopathy is depicted by the confusion matrices in Fig. 11.

Table VII: Mean Retinal Layers Segmentation Error

Layers	ILM	RNFL-GCL	IPL-INL	INL-OPL	ONL-IS	IS-OS	OS-RPE	Choroid
CSR	0.0045	0.0110	0.0328	0.0211	0.0820	0.0455	0.0954	0.0990
	0.0594	0.0498	0.0103	0.0268	0.0639	0.0096	0.0707	0.0838
	0.0559	0.0397	0.0014	0.0218	0.0836	0.0291	0.0904	0.1039
	0.0541	0.0461	0.0174	0.0295	0.0198	0.0102	0.0226	0.0310
	0.0460	0.0352	0.0050	0.0092	0.0543	0.0145	0.0597	0.0733
Mean	0.0440	0.0364	0.0134	0.0217	0.0607	0.0218	0.0678	0.0782
S.D	0.0202	0.0136	0.0110	0.0069	0.0232	0.0137	0.0260	0.0259
ME	0.0102	0.0111	0.0125	0.0269	0.0414	0.1352	0.0756	0.0725
	0.0122	0.0151	0.0075	0.0432	0.0245	0.1215	0.0614	0.0615
	0.0247	0.0203	0.0113	0.0492	0.0387	0.1580	0.0662	0.0632
	0.0518	0.0400	0.0561	0.0664	0.0605	0.1469	0.0861	0.0736
	0.0102	0.0111	0.0125	0.0269	0.0414	0.1352	0.0756	0.0725
Mean	0.0247	0.0216	0.0218	0.0465	0.0413	0.1404	0.0723	0.0677
S.D	0.0166	0.0111	0.0199	0.0141	0.0128	0.0136	0.0095	0.0054
Healthy	0.0500	0.0526	0.1764	0.0294	0.0361	0.4056	0.1552	0.1102
	0.0479	0.0219	0.1759	0.0264	0.0428	0.4134	0.1816	0.1609
	0.0546	0.0614	0.2427	0.0760	0.0391	0.4325	0.1695	0.1416
	0.0443	0.0237	0.2003	0.0177	0.0110	0.1413	0.1729	0.1522
	0.0555	0.0392	0.1874	0.0082	0.0336	0.4041	0.1260	0.1024
Mean	0.0505	0.0398	0.1965	0.0315	0.0325	0.3594	0.1610	0.1335
S.D	0.0042	0.0156	0.0247	0.0234	0.0112	0.1095	0.0195	0.0231

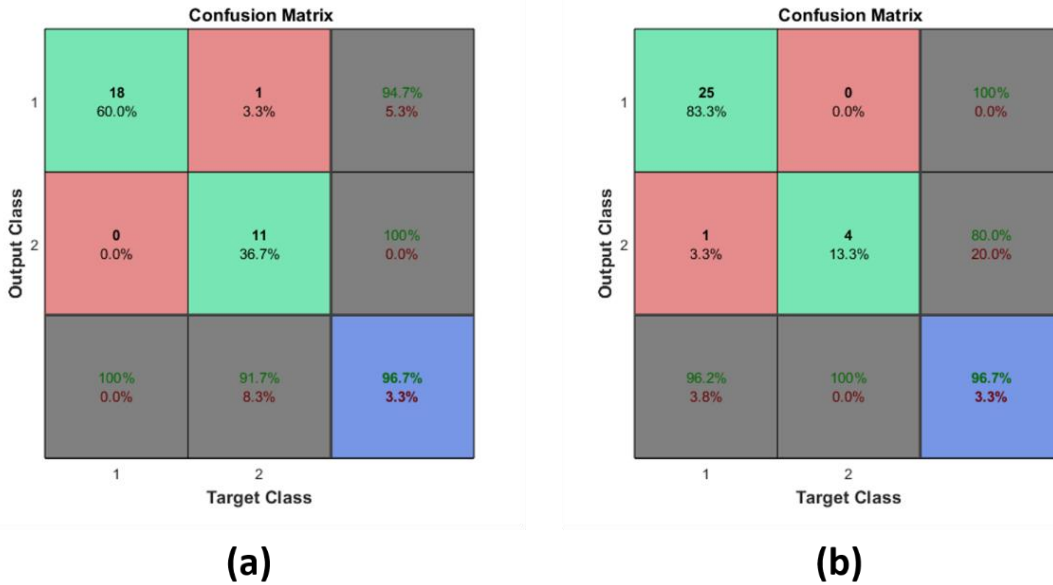


Fig. 11. Confusion matrices showing the performance of (a) ME Grading (b) CSR Grading

Fig. 12. shows some of the randomly selected samples from each case in which extracted ILM is shown in red color, extracted choroid is shown in purple color and fluid spaces are shown in cyan color.

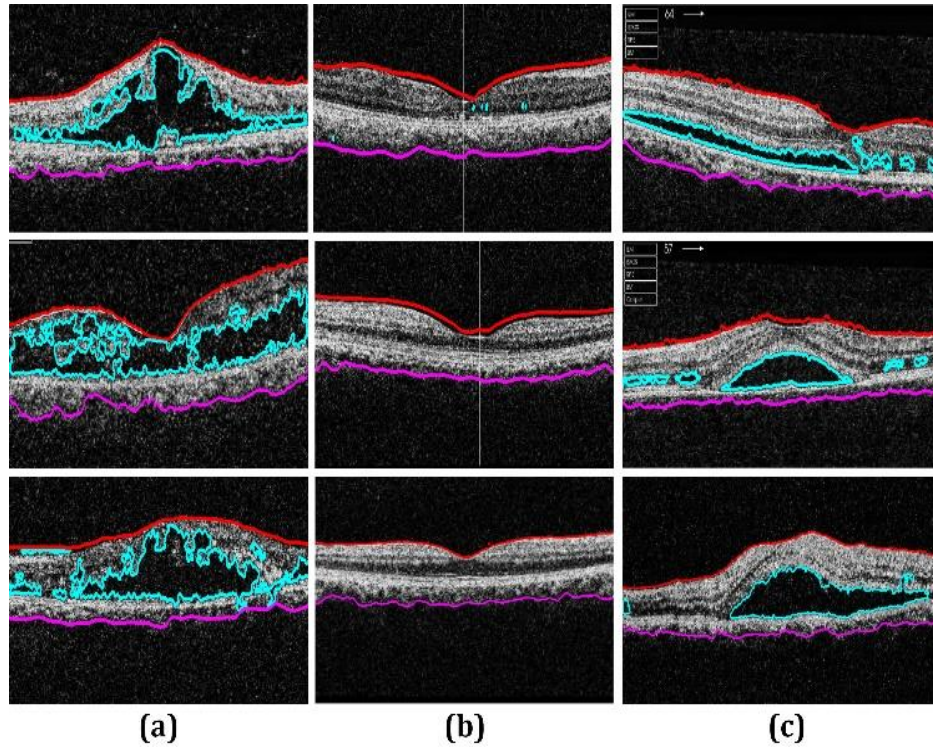


Fig. 12. Unlabeled Images (a) Diagnosed as ME, (b) Diagnosed as Normal, (c) Diagnosed as CSR.

4. DISCUSSION

We have proposed an automated system that can be used for the automated diagnosis and grading of ME, CSR and healthy pathology from OCT volumetric scans. ME and CSR are the macular disorders which are frequently associated with diabetes. These disorders mostly affect the young generation between 30-50 years. OCT is an eye testing technique which provides an objective evaluation of retinal pathology. Symptoms of retinal diseases appear at early stages in OCT scans. It is also possible to estimate the severity of retinal disorders from OCT imagery. The proposed system is based on novel ST-GS framework to extract intra-retinal layers and fluid pathology followed by the robust reconstruction of 3D retinal profiles from OCT scans. To the best of our knowledge, the proposed system is first of its kind that provide fully automated severity analysis of ME and CSR pathologies along with their grading as per clinical standards. Moreover, the performance of the proposed system is remarkable as shown in Table 6. The automated grading and 3D profiling of maculopathy takes one minute on average using 4th generation core i7 (1.8 GHz) processor with 8 GB RAM. The proposed system was tested on local dataset acquired from AFIO Rawalpindi where the proposed method correctly classified all of ME and CSR volumetric scans, although there were some noisy volumes in AFIO dataset as shown in Fig. 13.

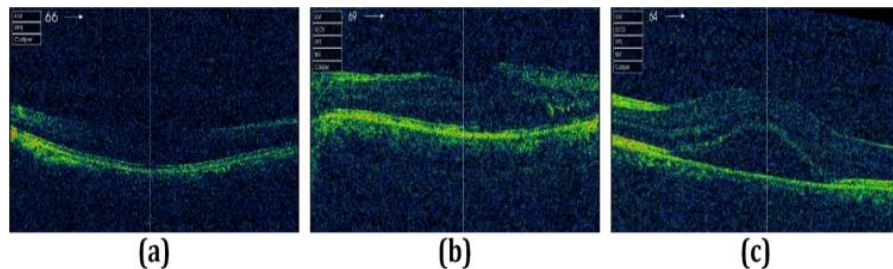


Fig. 13. Bad quality OCT B-scans (a) healthy (b) ME (c) CSR

In CSR, the fluid accumulates within RPE whereas neurosensory retina remains intact. In that case the cyst energy is quite low and we have discriminating values of f_5 , f_6 and f_7 as compared to ME in which we have irregular cyst spaces. In AFIO dataset, there are 5 ME cases which also have small CSR variations. Also, there are 2 CSR cases which have ME cysts as well. All of these cases are classified to ME and CSR class respectively because f_5 , f_6 and f_7 are more prone towards that class which has major symptoms in the scan. However, there is always a tradeoff between sensitivity and specificity but the proposed system correctly classified all diseased OCT scans without any false positive which is very significant. Also for the ME case, it is very difficult to accurately segment retinal layers due to the cyst fluid present in between them also shown in Fig 5(c). That's why we have tuned the proposed system more on accurately detecting the cyst fluid spaces rather than retinal layers because it provides a better estimation of ME severity as compared to retinal layers segmentation. Furthermore, the proposed system can provide an aid to ophthalmologists to mass screen retinal patients across different geographical areas of the world. Automatically generated 3D profiles and maculopathy grading reports from the proposed system can also support the diagnosis of ophthalmologists through quantitative numbers and standardize measures.

5. CONCLUSION

We present a novel OCT based clinical decision support system that can diagnose and grade ME and CSR. The proposed method relies on the robust generation of 3D retinal profiles and intra-retinal fluid through ST-GS based segmentation framework. Apart from this, the proposed system utilizes multilayered SVM classification model for the diagnosis of normal, ME and CSR subjects. The diseased candidates are further graded based upon the disease severity level. The proposed system was applied on the dataset consisting of 90 volumetric scans in which 60 of them are diseased (30 ME scans, 30 CSR scans) and the remaining 30 depicts healthy pathology. The dataset has been annotated by multiple ophthalmologists. The classification in the proposed framework is done by extracting a 7D feature vector from each candidate volumetric scan and passing it to the SVM based multi-classification system. After that the proposed system automatically measures the severity of the disease by grading it according to the clinical standards. Currently we have applied this system for the automated diagnosis and severity analysis of maculopathy. However, it can be used for the grading and 3D profiling of ocular diseases as well.

References

- [1] L. Conceicao, I. Pires, J. C. Vaz, "Diabetic Macular Edema", in *Optical Coherence Tomography: A Clinical and Technical Update*, 1st ed., Springer-Verlag Heidelberg, pp. 1–21, 2012.
- [2] N. Vukojevic, J. Sikic, D. Katusic and B. Saric. "Types of Central Serous Retinopathy, Analysis of Shape, Topographic Distribution and Number of Leakage Sites", *Collegium Antropologicum*, 25(1), pp. 83–87, June 2001.
- [3] T. Hassan, M. U. Akram, B. Hassan, A. Nasim, S. A. Bazaz, "Review of OCT and Fundus images for detecting Macular Edema", *IEEE 12th Int. Conference on Imaging Systems*, September 2015.
- [4] R. Z. Hannouche, M. P. Ávila, "Detection of diabetic foveal edema with bio microscopy, fluorescein angiography and optical coherence tomography", *Arquivos Brasileiros de Oftalmologia*, 71(5), pp. 759–763, October 2008.
- [5] W. Zhang, K. Yamamoto, S. Hori, "Optical Coherence Tomography for assessment of diabetic macular edema", *Int. Journal of Ophthalmology*, 1(4), pp. 370–373, September 2008.
- [6] A. Shrestha, N. Maharjan, A. Shrestha, R. Thapa, G. Poudyal, "Optical Coherence Tomographic assessment of macular thickness and morphological patterns in diabetic macular edema: Prognosis after modified grid photocoagulation", *Nepal Journal of Ophthalmology*, 4(7), pp. 128–133, February 2012.

- [7] N. F. Mokwa, T. Ristau, P. A. Keane, B. Kirchhoff, S. R. Sadda, S. Liakopoulos, "Grading of Age-Related Macular Degeneration: Comparison between Color Fundus Photography, Fluorescein Angiography, and Spectral Domain Optical Coherence Tomography", *Journal of Ophthalmology*, 2013, pp. 1–6, April 2013.
- [8] Y. M. Helmy, H. R. A. Allah, "Optical Coherence Tomography classification of diabetic cystoid macular edema", *Clinical Ophthalmology - Dove press*, 2013(7), pp. 1731–1737, August 2013.
- [9] D. Ferrara, K. J. Mohler, N. Waheed, M. Adhi, J. J. Liu, I. Grulkowski, M. F. Kraus, C. Bauml, J. Hornegger, J. G. Fujimoto, J. S. Duker, "En Face Enhanced-Depth Swept-Source Optical Coherence Tomography Features of Chronic Central Serous Chorioretinopathy", *American Academy of Ophthalmology*, 121(3), pp. 719–726, March 2014.
- [10] J. S. Wani, P. A. Bhat, A. Ahangar, S. Ismail, "Role of Optical Coherence Tomography in Central Serous Chorioretinopathy", *Journal of Evolution of Medical and Dental Sciences*, 4(45), pp. 7801–7809, June 2015.
- [11] M. Y. Teke, U. Elgin, P. N. Yuksekkaya, E. Sen, P. Ozdal, F. Ozturk, "Comparison of autofluorescence and optical coherence tomography findings in acute and chronic central serous chorioretinopathy", *Int J. Ophthalmol*, 7(2), pp. 350–354, April 2014.
- [12] C. Ahlers, W. Geitzenauer, G. Stock, I. Golbaz, U. S. Erfurth, C. Prunte, "Alterations of intraretinal layers in acute central serous chorioretinopathy", *Acta Ophthalmologica*, 87(5), pp. 511–516, August 2009.
- [13] K. Mitarai, F. Gomi, Y. Tano, "Three-dimensional optical coherence tomographic findings in central serous chorioretinopathy", *Graefe's Arch Clin Exp Ophthalmol*, 244(11), pp. 1415–1420, November 2006.
- [14] G. R. Wilkins, O. M. Houghton, A. L. Oldenburg, "Automated Segmentation of Intraretinal Cystoid Fluid in Optical Coherence Tomography", *IEEE Trans. on Biomedical Engineering*, 59(4), pp. 1109–1114, April 2012.
- [15] J. Sugruk, S. Kiattisin, A. L. Lasantitham, "Automated Classification between Age-related Macular Degeneration and Diabetic Macular Edema in OCT Image Using Image Segmentation", *IEEE Biomedical Engineering International Conference*, November 2014.
- [16] L. Zhang, W. Zhu, F. Shi, H. Chen, X. Chen, "Automated Segmentation of Intraretinal Cystoid Macular Edema for Retinal 3D OCT Images with Macular Hole", *International Symposium on Biomedical Imaging*, April 2015.
- [17] P. P. Srinivasan, L. A. Kim, P. S. Mettu, S. W. Cousins, G. M. Comer, J. A. Izatt, S. Farsiu, "Fully automated detection of diabetic macular edema and dry age-related macular degeneration from optical coherence tomography images", *Biomedical Optics Express*, 5(10), pp. 3568–3577, September 2014.
- [18] A. Rashno, D. D. Koozekanani, P. M. Drayna, B. Nazari, S. Sadri, H. Rabbani, K. K. Parhi, "Fully-Automated Segmentation of Fluid/Cyst Regions in Optical Coherence Tomography Images with Diabetic Macular Edema using Neutrosophic Sets and Graph Algorithms", *IEEE Transaction on Biomedical Imaging*, Volume PP, Issue 99, 31 July 2017.
- [19] A. M. Syed, T. Hassan, M. U. Akram, S. Naz, S. Khalid, "Automated diagnosis of macular edema and central serous retinopathy through robust reconstruction of 3D retinal surfaces", *Computer Methods and Programs in Biomedicine*, Volume 137, Pages 1–10, ISSN 0169-2607, December 2016.

[20] S. Khalid, M. U. Akram, T. Hassan, A. Nasim, and A. Jameel, "Fully Automated Robust System to Detect Retinal Edema, Central Serous Chorioretinopathy, and Age Related Macular Degeneration from Optical Coherence Tomography Images", BioMed Research International, Vol. 2017, Article ID 7148245, 15 pages, 2017. doi:10.1155/2017/7148245.

[21] B. Hassan, G. Raja, T. Hassan, M. U. Akram, "Structure Tensor Based Automated Detection of Macular Edema and Central Serous Retinopathy using Optical Coherence Tomography Images", Journal of the Optical Society of America A, USA, January 2016.

[22] T. Hassan, M. U. Akram, B. Hassan, A. M. Syed, and S. A. Bazaz, "Automated segmentation of subretinal layers for the detection of macular edema", Applied Optics, OSA. 55(3), pp. 454-461, January 2016.

J. S. Lim, "Image restoration," in Two-Dimensional Signal and Image Processing, 1st ed., Prentice-Hall, pp. 536-540, 1990.

[23] H. Knutsson, "Representing local structure using tensors", in Proc. of 6th Scandinavian Conference on Image Analysis, pp. 241-251, 1989.

R. E. Fan, K. W. Chang, C. J. Hsieh, X. R. Wang, C. J. Lin, "LIBLINEAR: A library for large linear classification", Journal of Machine Learning Research, 9(9), pp. 1871-1874, August 2008.

Deliverable: MATLAB API for edema detection

Results: The MATLAB module for macula edema detection and grading is completed.

Milestone 2: Conversion of preprocessing and layer segmentation Algorithms to high level language

The MATLAB API has been incorporated with the AL-BASR Application which enables the performing of OCT analysis.

Creation of MATLAB Dot Net API Library:

To enable MATLAB functionality to be used with-in the AL-BASR Application we have compiled a Dot Net API Dynamic Link Library (DLL) using the Compiler application available in the MATLAB.

Importing/Referencing of MATLAB DLL in the AL-BASR Application:

MATLAB DLL has to be imported/referenced inside the Windows Form Application of AL-BASR before its analysis performing functionality can be invoked. The MATLAB DLL is referenced in the application as an external resource.

Attaching of OCT images and Videos with the Patient's Case:

System allows the attachment of OCT Images and Videos to the patient case. A user can upload/attach the OCT files using the patient's visit interface. Ideally the OCT files are attached before or during a remote consultation session with a consultant present virtually via a video call.

Selection of OCT Video for Analysis:

User can select the OCT video file among other investigation files to start the analysis enabled via the MATLAB API. A user is presented with the analysis selection menu. After selecting an analysis the MATLAB API is invoked to start the analysis process. After completion of the process a PDF report of the results is displayed and stored along with the patient's record

Deliverable: Incorporation of Layer Segmentation API in windows form desktop application

Results:. Preprocessing and layer segmentation code designed in last quarter is successfully incorporated with EMR application.

Milestone 3: Adding data sharing and audio chatting capabilities in Telemedicine

Introduction:

Based on the database design and API achieved in the last milestone the telemedicine application has been developed that has the capability to allow referrals and remote consultations between physicians and patients. A remote consultation encounter/session is facilitated by patient medical record sharing and consultation over an audio/video call.

A telemedicine encounter can be initiated by a general practitioner to refer patient's case to an available consultant online. The consulting physician gets notified about the referral and access to the patient's case/visit is hence provided for the assessment. Initial record may include the subjective information mostly provided by the patient like the presenting complaint, history of present illness and vital signs. Patient's examination can be assisted by the consultant via the video call; system allows the consultant to order lab test or medications and an ability to view the results. After an assessment by the consultant a diagnosis can be entered along with follow up notes and the referral is finalized.

Tele-Consultation Session Flow of Events:

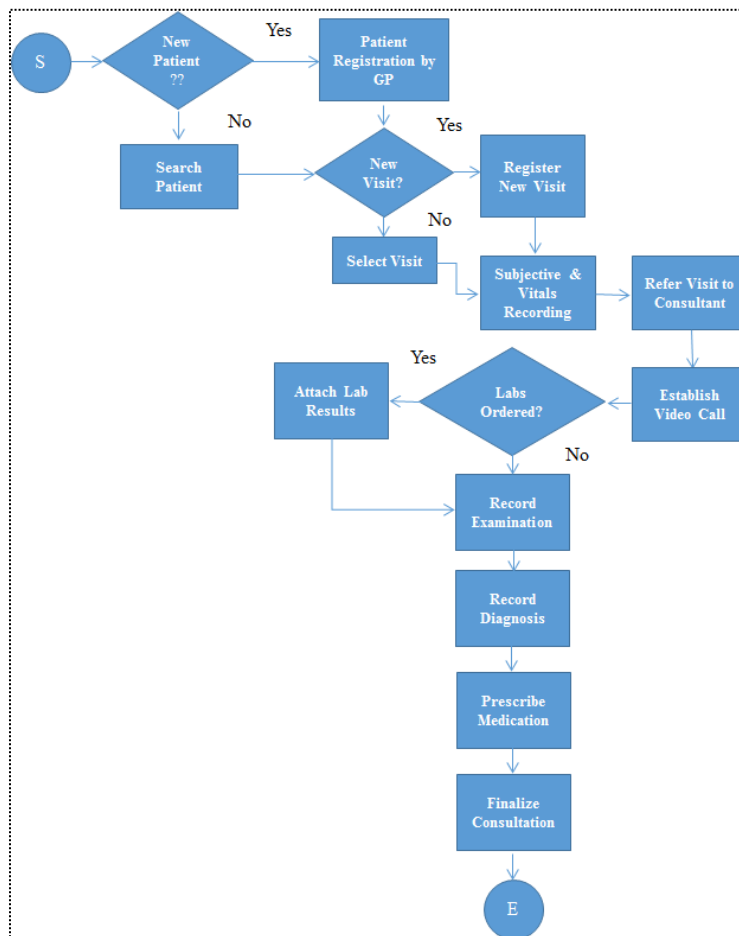


Figure 1 Tele-Consultation Workflow

1. Patient Registration:

The first step before any consultation can take place is the registration of the patient for whom the consultation is being required.

Following demographic information is taken at registration and a unique MRN # is allocated to the patient for identification:

1. Patient Name: First, Middle, Last
2. CNIC #
3. Date of Birth
4. Gender
5. Address
6. Contact Information: Phone, Email

After a successful registration a new patient record is created in the database. Every medical record kept/recorded in the future will be associated to the patient's profile.

2. Searching for an existing patient:

If the patient is already registered in the system, its record can be searched by giving in:

1. MR #
2. Patient Name
3. CNIC
4. Or any other field

List of possible patient matches are displayed to user, from which a required patient record may be selected.

3. Creation of a new Visit:

After a successful registration or search for a patient a new visit is recorded that registers that the patient has arrived for a consultation. A token number is allocated to the patient, which can be used to manage patient queues.

Starting of a visit marks the start of the patient's case; all activity will be tracked inside the visit, like the subjective notes, vital signs, examination, lab orders and results, medications and follow up notes. A visit record is actually shared when a patient is referred to a consultant.

4. Selection of an existing visit:

All visits recorded for the patient are accessible and so are displayed for selection; if an existing visit is to be selected, system allows it. After a visit selection the same clinical process can be conducted like in the case of a new visit.

5. Recording of Subjective Information:

Patient presents the chief complaint or the primary reason of the visit. The General Practitioner may enquire history of presenting illness and take vital signs. The system provides the capability to record subjective findings. The subjective notes assist the consultant in the examination and eventual diagnosis of the patient.

6. Referral to the Consultant:

After recording of the subjective assessment, patient's visit/case can now be referred to an available consultant. A list of available consultants is displayed. Referral can be made to a

consultant who appears in the list of available consultants. Consultant is notified about the referral. All clinical notes taken so far in the visit are shared to the referring consultant

7. Establishing of Video Call:

A video call can be requested by the General Physician. The referred consultant may be assisted by the General Physician via the call to conduct a thorough examination.

8. Order of Labs and Attaching of Results & Viewing:

System allows the referred consultant to order labs. The generated lab orders are communicated immediately to the General Practitioner who upon reception of lab results can attach them with patient's record.

The referred consultant is facilitated by the system to view the uploaded/attached lab results via a customized file-viewer integrated into the application.

9. Recording of Examination:

After have reviewed patient subjective information, lab results and conduction of remote physical examination assisted by the GP the referred consultant can now record examination notes. System provides the consultant the ability to write and format comprehensive notes.

10. Recording of a Diagnosis:

After assessing the patient medical state based on the notes taken, vital signs captured, labs ordered and examination conducted the consultant can now give diagnosis. System has kept a database of ICD-10 Complaint diagnoses. Consultant can type in and find the appropriate diagnosis to be recorded against the patient's state.

11. Recording of the care-plan:

After having given the diagnosis the consultant prescribes a care plan. A care plan includes the medications prescribed, there quantity, route of administration, dosage and frequency. As per requirement medications are added to the record. Follow up notes can also be associated with the plan.

12. Finalization of Consultation:

Prescribing and recording of a care plan marks the end of a consultation encounter and the referred consultant finalizes the visit.

Deliverable: Working telemedicine application having video & audio chatting and data sharing capabilities

Results: The milestone has been achieved.